Rotary propagation characteristics of light in multimode-single mode-multimode fiber structures using ray tracing method*

GAO Hong-yun (郜洪云), **WU Zi-wei** (吴紫薇), **XU Zhe-xiong-yan** (许哲雄言), **and LI Min** (黎敏)**
Department of Physics, Wuhan University of Technology, Wuhan 430070, China

(Received 4 June 2015)

The mode theory is the main way to study the propagation characteristics of light in fiber so far, but it is not suitable for analysis of light in duct. By using ray-tracing method, the rotary propagation characteristics of light in multimode-single mode-multimode (MSM) fiber structures are analyzed in this paper. Firstly, the light ray in fiber can propagate around an inscribed circle, and the central axis of this fiber is the propagation axis. Secondly, the radius of the inscribed circle is decided by both incident angle and incident position, and its variation is between 0 and R_M, where R_M is the radius of the multimode fiber. Lastly, the bigger the ratio of core and cladding diameter is, the higher the propagation efficiency is.

Document code: A **Article ID:** 1673-1905(2015)04-0294-4
DOI 10.1007/s11801-015-5105-z

In the applications of optical communication, sensing and detection, it is necessary to accurately describe the propagation characteristics of light in optical fiber. Because there are several special propagation modes for optical fibers, the mode theory attracts wide interest of researchers[1-3]. As far as we know, hollow duct and lens duct have been widely used in lasers[4,5]. However, the mode theory is not effective enough to analyze the propagation characteristics of light in duct. Ray-tracing method has been used to analyze the propagation characteristics of light for many optical systems[6-9]. But the researches are only concentrated on the radial light rays through the center axis[10,11]. It is well known that light rays propagating in optical fiber or duct include two parts of radial propagation and rotary propagation. Moreover, most of them are rotary propagation rays, and radial propagation is just a special condition of rotary propagation. So, we must study the rotary propagation characteristics of the light rays in order to gain real results.

Multimode-single mode-multimode (MSM) fiber structures have been concerned by a lot of researchers[12-14]. The propagation loss in MSM fiber structures has great influence on the sensitivity of fiber sensor, so it is necessary to analyze the propagation efficiency. In this paper, by using ray-tracing method, the rotary propagation characteristics of light rays in MSM fiber structures are studied, meanwhile, the propagation formula, the simulation results and the propagation efficiency are also given. The research methods and results are simple and clear, which can be used to analyze the propagation characteristics and rules of light rays in other optical fibers or ducts.

The schematic diagram of the MSM fiber structures is shown in Fig.1. It consists of two multimode fibers (MMFs) and one single mode fiber (SMF). Here, MMF1 is the former multimode fiber where the light is incident on the surface1 of the fiber core1, SMF is the middle single mode fiber, and MMF2 is the latter multimode fiber where the signal light is output from the end surface4. n_1, n_2 and n_3 are the refractive indices of MMF core, SMF cladding and MMF cladding, respectively, where MMF1 and MMF2 are the same. $2R_M$ and $2R_S$ are the diameters of MMF core and SMF cladding, respectively, where the claddings of MMF and SMF are the same. L_1, L_2 and L_3 are the lengths of MMF1, SMF and MMF2, respectively. The input light is incident on the planar surface1, which will be transmitted into SMF and output from the surface4 lastly. Because the core radius of SMF is much smaller than those of MMFs, the calculations in the following do not take those light rays without any reflection into account.

The schematic diagram of a three-dimensional cylindrical coordinate system of MSM fiber is shown in Fig.2. Here, the center of surface1 is the origin O of the coordinate system, the central axis of the fiber is the x-axis, and the y-axis and the z-axis are horizontal and vertical, respectively. Supposing a light ray is incident on the planar surface1 from the point A_0 with the initial coordi-

* This work has been supported by the National Natural Science Foundation of China (No.61177076), and the Fundamental Research Funds for the Central Universities (Nos.2013-Ia-038 and 2013-Ia-006).
** E-mail: minli@whut.edu.cn

nate of (x_0, 0, 0), $A_1(R_M, \gamma_1, l_1)$ is the first total reflection point of the considered ray. γ_1 is the rotation angle formed by the back intersecting point with respect to the former point in the *X*-*Y* projection plane, and it is positive if the ray is anticlockwise with respect to the *z*-axis. l_1 is the propagation length of the light along the *z*-axis. α_1 is the propagation angle in MMF1, which means the angle between the incident light and the *z*-axis, and t_1 is the projection length of the incident ray from surface1 to the first total reflection point in the *X*-*Y* projection plane.

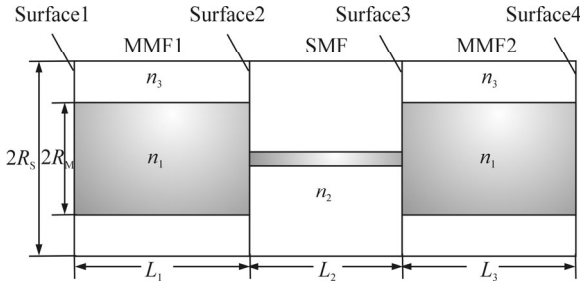

Fig.1 The schematic diagram of MSM fiber structures

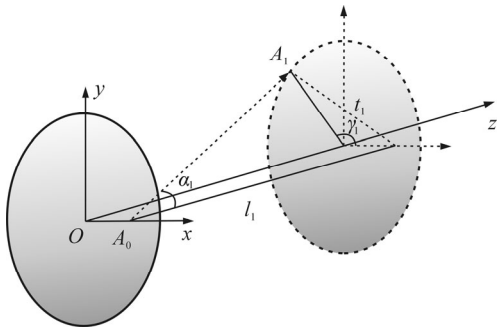

Fig.2 The three-dimensional cylindrical coordinate system

The total reflection condition of the incident light can be calculated as

$$\sin\alpha_1 \le \frac{t_1\sqrt{1-\frac{n_3^2}{n_2^2}}}{R_M - x_0\cos\gamma_1}, \tag{1}$$

where

$$t_1 = \sqrt{(R_M\cos\gamma_1 - x_0)^2 + (R_M\sin\gamma_1)^2}\ . \tag{2}$$

The propagation rule of the light in the MSM fiber structures can be divided into three parts as follows.

Firstly, the incident ray in MMF1 can propagate around an inscribed circle with radius of *r*, where

$$r = \frac{x_0 R_M\sin\gamma_1}{t_1}\ . \tag{3}$$

So the projection of the ray in the *X*-*Y* projection plane remains tangent to the inscribed circle whose center is on the *z*-axis, as shown in Fig.3.

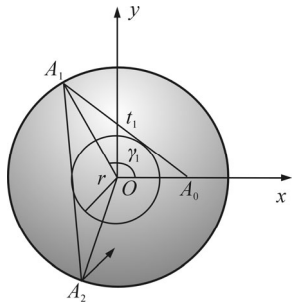

Fig.3 The projection of incident ray in MMF1

The coordinates of the total reflection points $A_n(\rho, \theta, z)$ of light rays in MMF1 can be expressed as $(R_M, \gamma_1 + 2(n-1)\arccos\frac{r}{R_M}, \frac{t_1 + 2(n-1)\sqrt{R_M^2 - r^2}}{\tan\alpha_1})$, $(n=1,2,\cdots,N)$, where *n* is the order of the intersecting points of incident ray in MMF1. When the propagation length is equal to L_1, we can have

$$N = \left[\frac{L_1\tan\alpha_1 - t_1}{2\sqrt{R_M^2 - r^2}} + 1\right]. \tag{4}$$

Secondly, the incident ray in SMF can propagate around the former inscribed circle whose radius is still *r*, as shown in Fig.4.

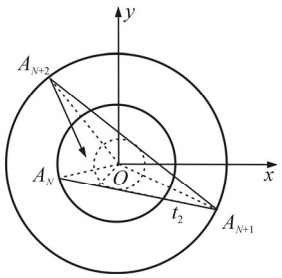

Fig.4 The projection of incident ray in SMF

From Snell's law, the propagation angle α_2 in SMF can be calculated by

$$\alpha_2 = \arcsin(\frac{n_1\sin\alpha_1}{n_2})\ . \tag{5}$$

The coordinates of total reflection points $A_{N+m}(\rho, \theta, z)$ of incident ray in SMF can be expressed as $(R_S, \gamma_1 + (2N-1)\times\arccos\frac{r}{R_M} + (2m-1)\arccos\frac{r}{R_S}, L_1 + \frac{t_2 + 2(m-1)\sqrt{R_S^2 - r^2}}{\tan\alpha_2})$, $(m=1,2,\cdots,M)$, where t_2 is the projection length of the incident ray from surface2 to the first total reflection point A_{N+1} in SMF, and *m* is the order of the intersecting points of propagation ray in SMF. Then we can have

$$t_2 = t_1 - L_1\tan\alpha_1 + \sqrt{R_S^2 - r^2} + (2N-1)\sqrt{R_M^2 - r^2}\ , \tag{6}$$

$$M = \left[\frac{L_2\tan\alpha_2 - t_2}{2\sqrt{R_S^2 - r^2}} + 1\right]. \tag{7}$$

And lastly, the incident ray inside MMF2 will propagate around an inscribed circle with radius of r, as shown in Fig.5. The propagation angle of the incident ray is α_1.

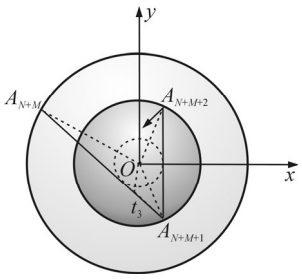

Fig.5 The projection of incident ray in MMF2

Here, the propagation rays in MMF2 must meet the following condition of

$$\sqrt{R_S^2-r^2}-\sqrt{R_M^2-r^2}<L_2\tan\alpha_2-t_2-2(M-1)\sqrt{R_S^2-r^2}<\sqrt{R_S^2-r^2}+\sqrt{R_M^2-r^2} \quad . \tag{8}$$

The coordinates of the total reflection points $A_{N+M+q}(\rho, \theta, z)$ of incident rays in MMF2 can be expressed as $(R_M, \gamma_1+2M\arccos\frac{r}{R_S}+2(q+N-1)\arccos\frac{r}{R_M}, L_1+L_2+\frac{t_3+2(q-1)\sqrt{R_M^2-r^2}}{\tan\alpha_1})$, $(q=1,2,\cdots,Q)$, where t_3 is the projection length of the incident ray from surface3 to the first total reflection point A_{N+M+1} in MMF2, and q is the order of the intersecting points of the propagation ray in MMF2. Then we can have

$$t_3=t_2-L_2\tan\alpha_2+\sqrt{R_M^2-r^2}+(2M-1)\sqrt{R_S^2-r^2} \quad , \tag{9}$$

$$Q=\left[\frac{L_3\tan\alpha_1-t_3}{2\sqrt{R_M^2-r^2}}+1\right]. \tag{10}$$

Fig.6 shows the calculated simulation results of one incident ray in MMF1, where Fig.6(a) and (b) are the schematic diagrams of propagation and projection, respectively. From Fig.6 we can conclude that this single incident ray can always propagate around an inscribed circle in MMF1, and the radius of the inscribed circle is constant.

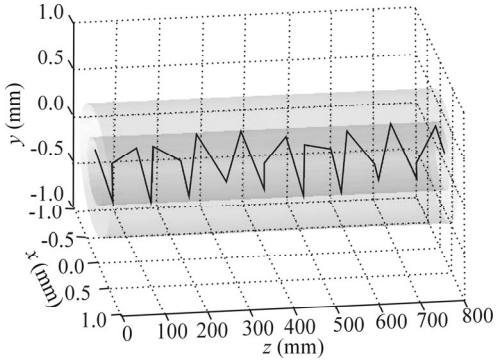

(a) Schematic diagram of propagation

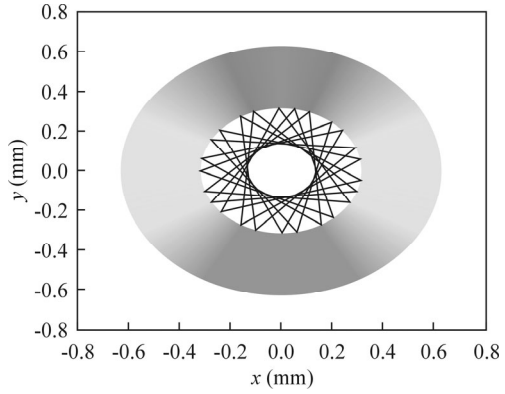

(b) Schematic diagram of projection

Fig.6 The calculated simulation results of one incident ray in MMF1

Fig.7 shows the calculated simulation results of one incident ray in MSM fiber structures. From Fig.7(b), we can conclude that this single incident ray can always propagate around an inscribed circle, and the radius of the inscribed circle is constant.

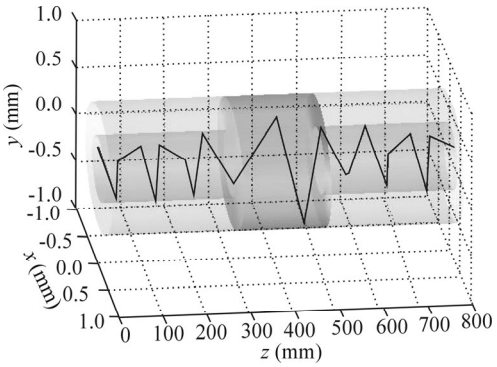

(a) Schematic diagram of propagation

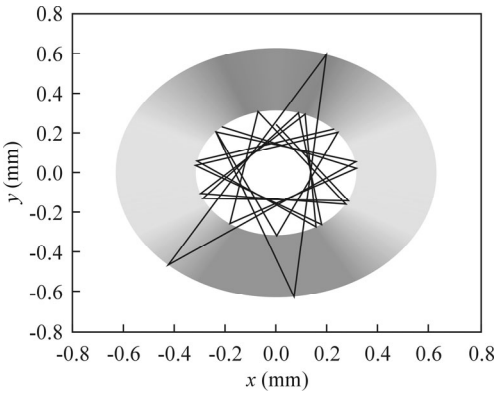

(b) Schematic diagram of projection

Fig.7 The calculated simulation results of one incident ray in MSM fiber

Fig.8 shows the calculated simulation results of three incident rays in MSM fiber structures. From Fig.8(b), we can conclude that the three incident rays can always propagate around three different inscribed circles, and the radii of the three inscribed circles are also constant.

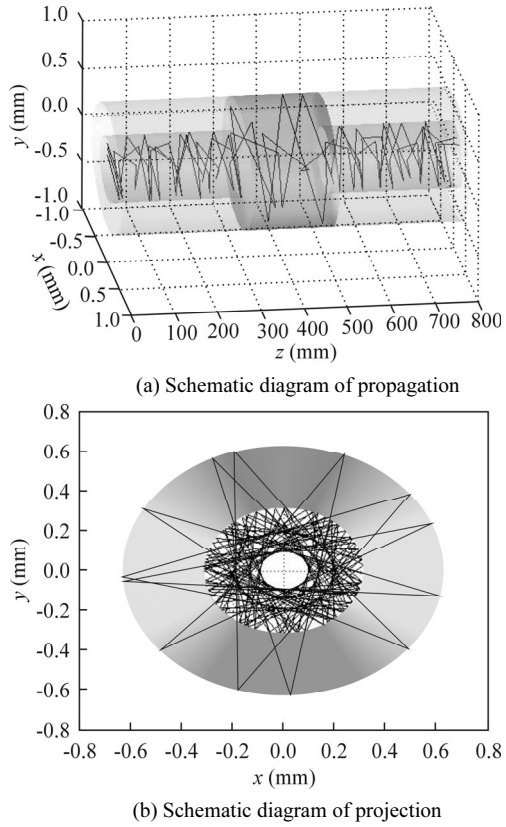

(a) Schematic diagram of propagation

(b) Schematic diagram of projection

Fig.8 The calculated simulation results of three incident rays in MSM fiber structures

Fig.9 shows the simulation result of propagation efficiency of incident rays in MSM fiber structures, namely, the relationship between propagation efficiency and ratio of core and cladding diameters of MMF (D_M/D_S), where n_1, n_2, n_3, L_1, L_2 and L_3 are 1.468 1, 1.462 8, 1.462 8, 200 mm, 10 mm and 200 mm, respectively. So it can be concluded that the bigger the ratio is, the higher the propagation efficiency is.

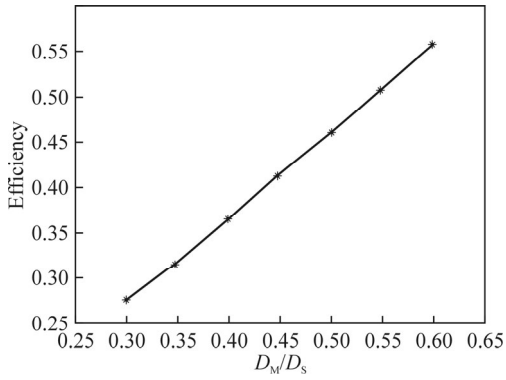

Fig.9 The relationship between propagation efficiency and the ratio of core and cladding diameters

Thus, we can know from the above analyses that different rotary rays in MSM fiber structures will propagate around different inscribed circles, the radius of inscribed circle is decided by the incident angle and incident position, and the variation of inscribed circle radius is between 0 and R_M. These conclusions can be used to analyze the propagation rule and characteristics of light rays in arbitrary ordinary optical fiber, duct and other optical waveguide by using the principle of total reflection. However, it is necessary to point out that the ray-tracing method is based on the theory of total internal reflection principle, and it doesn't consider the propagation mode in optical fiber. For the reason, by using this kind of analysis way in this paper, the propagation efficiency is higher than the real value.

In summary, we investigate the rotary propagation characteristics of light in MSM fiber structures by using ray-tracing method and computer simulation in this paper. The propagation formulas and rules are proposed completely. An incident ray in fiber can propagate around an inscribed circle until it is output to the next fiber or other medium. The variation of inscribed circle radius, which is decided by incident angle and position of light ray, is between 0 and the radius of fiber core. For MSM fiber structures, the bigger the ratio of core and cladding diameters is, the higher the propagation efficiency is. The simple and clear results are effective references for the analysis of light propagation characteristics in optical fiber, hollow duct, lens duct and other optical waveguide.

References

[1] Junhe Zhou, Optics Express **22**, 10815 (2014).

[2] Andrey A. Sukhorukov, Alexander S. Solntsev, Sergey S. Kruk, Dragomir N. Neshev and Yuri S. Kivshar, Optics Letters **39**, 462 (2014).

[3] Takeshi Fujisawa and Masanori Koshiba, Applied Optics **45**, 4114 (2006).

[4] Marc Eichhorn, Applied Optics **47**, 1740 (2008).

[5] Carlito S. Ponseca, Elmer Estacio, Romeric Pobre, Gilbert Diwa, Glenda de los Reyes, Shingo Ono, Hidetoshi Murakami, Nobuhiko Sarukura, Ko Aosaki, Yoshihiko Sakane, Hideki Sato, Alexander Argyros and Maryanne C. J. Large, Journal of the Optical Society of America B **26**, A95 (2009).

[6] Ichikawa Tsubasa, Yoneyama Takuo and Sakamoto Yuji, Optics Express **21**, 32019 (2013).

[7] Hong-Yun Gao, Ru-Lian Fu, Zhao-Qi Wang and Xin-Gang Shi, Optics Communications **260**, 699 (2006).

[8] Yohei Nishidate, Takashi Nagata, Shin-ya Morita and Yutaka Yamagata, Applied Optics **50**, 5192 (2011).

[9] Tsubasa Ichikawa, Takuo Yoneyama and Yuji Sakamoto, Optics Express **21**, 32019 (2013).

[10] DI Hai-ting and FU Yi-li, Journal of Optoelectronics·Laser **25**, 1092 (2014). (in Chinese)

[11] ZHUANG Lin-ling, ZHUANG Qi-ren, CHEN Chun-yu, WANG Ju-feng, HU Yi-bin and LIU Shi-wei, Journal of Optoelectronics·Laser **25**, 1892 (2014). (in Chinese)

[12] A. Hosoki, M. Nishiyama, H. Igawa, Y. Choi and K. Watanbe, Procedia Engineering **47**, 128 (2012).

[13] Keiju Takagi and Kazuhiro Watanabe, Sensors **12**, 2208 (2012).

[14] Ai Hosoki, Michiko Nishiyama, Hirotaka Igawa, Atsushi Seki, Yongwoon Choi and Kazuhiro Watanabe, Sensors and Actuators B: Chemical **185**, 53 (2013).